⌘ *Author's Choice*

THE JOURNAL OF BIOLOGICAL CHEMISTRY VOL. 284, NO. 51, pp. 35916–35925, December 18, 2009

Sensing Domain Dynamics in Protein Kinase A-Iα Complexes by Solution X-ray Scattering*

Received for publication, August 27, 2009 Published, JBC Papers in Press, October 15, 2009, DOI 10.1074/jbc.M109.059493

Cecilia Y. Cheng[‡], Jie Yang[‡], Susan S. Taylor[‡§], and Donald K. Blumenthal[¶1]

From the Departments of [‡]Chemistry and Biochemistry and [§]Pharmacology and the Howard Hughes Medical Institute, University of California, San Diego, La Jolla, California 92037-0654 and the [¶]Department of Pharmacology and Toxicology, University of Utah, Salt Lake City, Utah 84112

The catalytic (C) and regulatory (R) subunits of protein kinase A are exceptionally dynamic proteins. Interactions between the R- and C-subunits are regulated by cAMP binding to the two cyclic nucleotide-binding domains in the R-subunit. Mammalian cells express four different isoforms of the R-subunit (RIα, RIβ, RIIα, and RIIβ) that all interact with the C-subunit in different ways. Here, we investigate the dynamic behavior of protein complexes between RIα and C-subunits using small angle x-ray scattering. We show that a single point mutation in RIα, R333K (which alters the cAMP-binding properties of Domain B) results in a compact shape compared with the extended shape of the wild-type R·C complex. A double mutant complex that disrupts the interaction site between the C-subunit and Domain B in RIα, RIα_{AB}R333K·C(K285P), results in a broader $P(r)$ curve that more closely resembles the $P(r)$ profiles of wild-type complexes. These results together suggest that interactions between RIα Domain B and the C-subunit in the RIα·C complex involve large scale dynamics that can be disrupted by single point mutations in both proteins. In contrast to RIα·C complexes. Domain B in the RIIβ·C heterodimer is not dynamic and is critical for both inhibition and complex formation. Our study highlights the functional differences of domain dynamics between protein kinase A isoforms, providing a framework for elucidating the global organization of each holoenzyme and the cross-talk between the R- and C-subunits.

cAMP is an important second messenger responsible for the conversion of an extracellular stimulus into a cascade of intracellular signaling events. The primary sensor for cAMP in mammalian cells is cAMP-dependent protein kinase (PKA).[2] PKA is a ubiquitous Ser/Thr kinase that phosphorylates numerous proteins, eliciting diverse biological responses including learning, memory (1), metabolism (2), and cell death (3). In the absence of cAMP, PKA is an inactive tetramer composed of two catalytic (C) subunits bound to a dimer of regulatory (R) subunits. Binding of two cAMP molecules to each R-subunit releases two catalytically active C-subunits.

There are four PKA R-subunit isoforms (RIα, RIβ, RIIα, and RIIβ), and all share the same domain organization. All of the R-subunits contain an N-terminal dimerization/docking domain that interacts with anchoring proteins, an inhibitor sequence that binds to the C-subunit active site, and two tandem cAMP-binding domains (designated Domains A and B). Despite these commonalities, each isoform differs in its cellular and tissue-specific distribution, abundance, sequence, structure, and biochemical properties. Moreover, each isoform is functionally nonredundant. Only RIα subunits are embryonically lethal (4, 5), and mutations in RIα are associated with Carney complex (6–8) and systemic lupus erythematosus (9, 10). Given the biological differences between the PKA isoforms and their relevance to disease, it is important to characterize their molecular properties more rigorously to better understand their functional differences.

The PKA-Iα holoenzyme crystal structure described by Kim *et al.* (11) illuminated the detailed interactions between the C- and RIα-subunits and elucidated a molecular mechanism for the ordered and cooperative activation of PKA by cAMP. Both the structure and mutational data highlighted the role of Domain B as the gatekeeper domain for Domain A. cAMP first binds to Domain B, triggering a conformational change that enables cAMP to bind to Domain A. This second cAMP binding step releases the active C-subunits (12). The first conformational change in RIα involves reorientation of the two cAMP-binding domains, induced by structural changes in the αB and αC helices connecting Domains A and B (Fig. 1). In the C-subunit-bound conformation, the αB and αC helices combine to form a single contiguous helix (αB/C), producing an overall dumbbell-shaped structure where the two domains are separated (Fig. 1*A*, *left panel*). In the cAMP-bound conformation, the αB/C helix is divided into three sections, producing an overall compact globular structure where the two domains share a common interface (Fig. 1*A*, *right panel*). Fig. 1*B* compares the changes in the αB and αC helices when RIα shuttles between the cAMP-bound and C-subunit-bound conformations. In the cAMP-bound conformation, the αB and αC helices form distinct segments with residues Gly^{235} and Tyr^{244} serving as two hinge points. In contrast, these same two residues are engaged to form the continuous helix in the C-subunit-bound conformation. These structural comparisons highlight the dynamic nature of the two domains within the RIα-subunit and show that the conformational transition between the active (cAMP-

* This work was supported, in whole or in part, by National Institutes of Health Grants GM34921 (to S. S. T.) and GM08326 (to C. Y. C.). This work was also supported in part by American Heart Association (Western States Affiliate) Grant 07015019Y (to C. Y. C.).

⌘ *Author's Choice*—Final version full access.

[1] To whom correspondence should be addressed: 112 Skaggs Hall, Salt Lake City, UT 84112. Tel.: 801-585-3094; Fax: 801-585-5111; E-mail: Don.Blumenthal@pharm.utah.edu.

[2] The abbreviations used are: PKA, protein kinase A; C-subunit, catalytic subunit; R-subunit, regulatory subunit; SAXS, small angle x-ray scattering; MOPS, 4-morpholinepropanesulfonic acid.

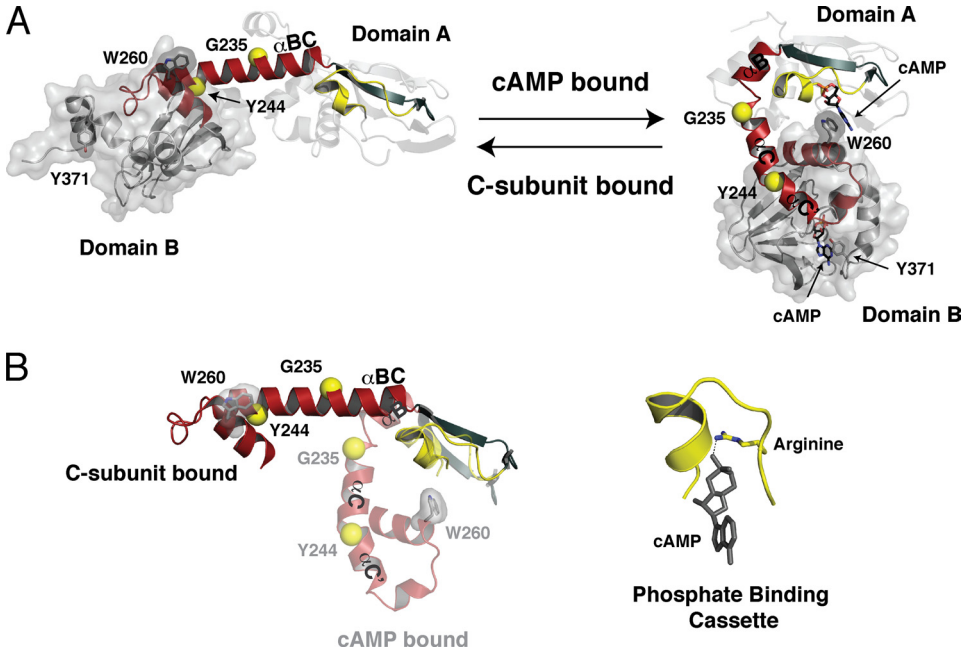

FIGURE 1. *A*, conformational change of RIα upon binding to the C-subunit (*left*) and cAMP (*right*). The connecting αB and αC helices are shown in *red*, and the two hinge points are highlighted with *yellow spheres*. Domain B is rendered in surface representation for clarity. *B*, *left*, overlay of αB and αC helices in the C-subunit and cAMP-bound conformations. *Right*, the phosphate-binding cassette highlighting the role of a critical arginine (Arg^{209} for Domain A and Arg^{333} for Domain B) binding to the phosphate of cAMP. The phosphate-binding cassette is colored in *yellow* in *A* and *B*.

bound) and inactive (C-subunit-bound) states consists of large scale domain motions around two hinge points.

During efforts to crystallize the PKA-Iα holoenzyme complex, parallel crystallization trials were set up for three RIα deletion mutants ($RI\alpha_{AB}$, $RI\alpha_{AB}$R209K, and $RI\alpha_{AB}$R333K, where $RI\alpha_{AB}$ refers to the truncated form of $RI\alpha_{91-379}$ containing both cAMP-binding domains) in complex with the C-subunit. Only the holoenzyme formed with $RI\alpha_{AB}$R333K produced crystals that diffracted to 2.2 Å. Arg^{333} is essential for high affinity binding of RIα to cAMP in Domain B (the corresponding residue in Domain A is Arg^{209}). This residue is located within the phosphate-binding cassette of RIα (residues 199–211 and 323–335 for Domains A and B, respectively), and its side chain forms a hydrogen bond with the cAMP phosphate (Fig. 1*B*, *right panel*). The R333K mutation was first identified in S49 mouse lymphoma cells (13) and was shown to diminish the ability of PKA to respond to cAMP (14). Our study addresses the effects of the R333K mutation on the global architecture of the RIα·C complex in solution.

Previous small angle x-ray scattering (SAXS) data showcased differences in the overall shape of holoenzymes formed with truncated RI- and RII-subunits (15–17). In these R-subunit constructs, the N-terminal dimerization domains were removed so that only R·C heterodimers were monitored. The RIIα·C and RIIβ·C heterodimers formed compact, globular particles, whereas the RIα·C heterodimer exhibited a more elongated shape that produced a $P(r)$ curve with a broad shoulder in the high r region. Although the source of the extended tail has not been unequivocally determined, we hypothesize that it is due to extension of a highly dynamic Domain B in RIα (18).

Here, we focus on four main questions: 1) In the RIα $P(r)$ curve, is the shoulder at the high r region due to Domain B? 2) Is the large scale domain organization of RIα altered within the R·C complex when mutations are introduced into either Domain A or B? 3) Can mutations at particular sites in the C-subunit be utilized to disrupt a specific interface in the R·C complex, and can SAXS detect these changes? 4) Finally, can we interpret and account for the SAXS differences between RI- and RII-subunits as a result of variations in the overall organization of the cAMP-binding domains and/or differences in the cross-talk between the R- and C-subunits? Answers to these questions should provide insights into how the diversity between R-subunit isoforms give rise to the unique and sophisticated mechanisms of isoform-specific PKA regulation in cells.

To test our hypothesis that Domain B in PKA-Iα is highly flexible and the effects of the R333K mutation on this flexibility, we utilized a combination of site-directed mutagenesis, biochemical analysis, and small angle x-ray scattering to better understand the role of Domain B dynamics in PKA-Iα complexes. The SAXS results reported here show that heterodimers formed with the $RI\alpha_{AB}$R333K mutant display a different SAXS profile from wild-type $RI\alpha_{AB}$ and that these differences stem from Domain B. Our data also indicate that in RIα, Domain B is dynamic even when complexed with the C-subunit. In contrast to RIIβ where Domain B is essential for C-subunit interactions, the interaction of Domain B from RIα with the C-subunit is dispensable for holoenzyme formation.

EXPERIMENTAL PROCEDURES

Protein Preparation—The catalytic subunit was expressed and purified in *Escherichia coli* BL21 (DE3) cells (Novagen) as described previously (19). Expression and purification of the C-subunit mutant K285P followed the same protocol. All of the RIα proteins ($RI\alpha_{A}$, $RI\alpha_{AB}$, $RI\alpha_{AB}$R209K, and $RI\alpha_{AB}$R333K, where $RI\alpha_{A}$ and $RI\alpha_{AB}$ refers to constructs corresponding to residues 91–244 and 91–379, respectively) were expressed and purified as described previously (20).

Holoenzymes of RIα mutants ($RI\alpha_{A}$, $RI\alpha_{AB}$, $RI\alpha_{AB}$R209K, and $RI\alpha_{AB}$R333K) were formed by mixing each R-subunit with wild-type C-subunit in a 1:1.2 molar ratio and then dialyzing overnight at 4 °C in 10 mM MOPS (pH 7.0), 50 mM NaCl, 2 mM $MgCl_2$, 2 mM dithiothreitol, and 0.5 mM ATP. Each holoenzyme complex was separated from excess C-subunit by gel filtration chromatography. Care was taken to concentrate samples immediately prior to SAXS data collection because these complexes were extremely prone to aggregation at concentrations higher than 5 mg/ml.

SAXS Data Collection—Small angle x-ray scattering measurements were collected at the University of Utah with an Anton Paar SAXSess instrument with line collimation and an image plate detector. The protein samples were concentrated to 2–5 mg/ml and filtered (0.22 μm) immediately prior to data collection. Scattering data for protein samples and their respective solvent blanks were collected in a 1-mm diameter quartz capillary with a 10-mm beam slit at 12 °C.

SAXS Data Analysis—Normalized buffer subtraction and data reduction to $I(q)$ *versus* q (where $q = (4\pi \sin\theta)/\lambda$, 2θ is the scattering angle, and λ is the wavelength of radiation, 1.54 Å) were performed with the program SAXSquant1D (Anton-Paar, Austria). Radius of gyration (R_g) and zero angle scattering ($I(0)$) parameters were calculated using both GNOM (21) and by Guinier analysis with the program PRIMUS (22). Inverse Fourier transform calculations of $I(q)$ to yield $P(r)$ functions, $I(0)$, R_g, and the maximum dimension (D_{max}) were carried out using a q range of 0.013–0.17 1/Å. CRYSOL was used to calculate theoretical scattering intensity from Protein Data Bank coordinates of R·C crystal structures (23). The figures were made in PyMOL (DeLano Scientific LLC, San Carlos, CA).

Amino Acid Analysis—Amino acid composition of each R·C complex was determined after SAXS data collection to accurately quantify protein concentrations. Amino acid analysis was performed by Dr. Dennis Winge at the University of Utah. The molecular weight (MW) of each complex was determined experimentally with the relation $I(0) = \propto^{*}MW^{2*}c$, where $I(0)$ is the scattering at zero angle, $\propto$ is a proportionality constant, and c is the concentration as determined by amino acid analysis. $I(0)$ was determined by GNOM, and the proportionality constant, $\propto$, was determined using lysozyme as a protein standard.

Structural Models—Ab initio shape restoration with the program DAMMIF (24) was used to generate three-dimensional structures from the one-dimensional scattering data of all seven PKA complexes. No symmetry constraints were applied, and default parameters were used in each calculation. Ten independent models for each heterodimer complex were generated, then aligned, and averaged using the program DAMAVER (25). DAMMIF models for RIα$_A$·C and RIα$_{AB}$R333K·C complexes were aligned with their respective crystal structure coordinates (Protein Data Bank codes 3FHI and 2QCS, respectively) using the program SUPCOMB (26).

Determination of Binding Kinetics by Surface Plasmon Resonance—Binding experiments were performed on a Biacore 3000 instrument (GE Healthcare). Purified wild-type and K285P mutant C-subunits were diluted to 10–50 μg/ml in 10 mM potassium phosphate buffer (pH 6.0), 20 mM NaCl, 1 mM ATP, and 10 mM $MgCl_2$. These proteins were immobilized onto CM5 Sensor Chips (GE Healthcare) via amine coupling to a ligand density response of ~300 response units (RU). Dilutions of RIα$_{AB}$ ranging from 0.5 to 250 nM were prepared in 10 mM HEPES (pH 7.4), 150 mM NaCl, 0.0005% (v/v) surfactant P-20 (HBS-P buffer; GE Healthcare), 1 mM dithiothreitol, 1 mM ATP, and 10 mM $MgCl_2$. Each RIα concentration was injected into the channels at a flow rate of 50 μl/min. The surface was regenerated with 200 μM cAMP and 2 mM EDTA in HBS-P buffer. Sensograms were analyzed using Biaevaluation software version 4.1 (GE Healthcare) to obtain kinetic parameters. Sensogram curves were fit to a 1.1 binding model.

Inhibition of C-subunit by RIα—The inhibition assay was carried out as described earlier (27). Briefly, C-subunit wild-type or K285P mutant proteins were incubated with varying concentrations of RIα$_{AB}$ for 30 min at 30 °C. Each reaction mix contained 0.5–1 mM of the substrate peptide Kemptide (LRRASLG), 1–2 nM C-subunit, and 0.5 mM ATP. R-subunit was serially diluted to final concentrations ranging from 0.5 to 500 nM. The reactions were initiated with a mixture of Kemptide, ATP, and [γ-^{32}P]ATP, allowed to proceed for 20 min at 30 °C, and then quenched with 30% acetic acid. Free [γ-^{32}P]ATP was separated from protein-bound radioactivity by ascending chromatography on phosphocellulose p81 Whatman paper as described previously (28). Phosphate incorporation into Kemptide was detected by Cerenkov counting on a Beckman LS 6000SC liquid scintillation system. Curve fitting and IC_{50} calculations were performed using GraphPad Prism 5 software (GraphPad, San Diego, CA).

RESULTS

SAXS data were collected for seven PKA-Iα holoenzyme complexes formed with a combination of four different RIα mutants (termed RIα$_A$, RIα$_{AB}$, RIα$_{AB}$R333K, and RIα$_{AB}$R209K) and two C-subunit proteins (wild type and K285P mutant; the RIα$_{AB}$R209K·C(K285P) complex was not examined). To study the contribution of the two cAMP-binding domains on PKA-Iα dynamics, we used RIα constructs RIα$_{91–244}$ and RIα$_{91–379}$, which lacked the N-terminal dimerization domain and the linker region. The minimal sequence required to form a high affinity complex with the C-subunit includes the inhibitor sequence region (residues 91–100) and Domain A (residues 120–244). The SAXS intensity plots of $I(q)$ *versus* q, Guinier plots, and associated distance distribution $P(r)$ functions are shown in Figs. 2 and 3. Guinier plots for all samples were linear at the low q range, indicative of monodisperse solutions with no presence of nonspecific aggregation during data acquisition. Because each sample contained monodisperse particles, these data were suitable for structural analysis. The intensity curves were fit, and inverse Fourier transforms were performed using the program GNOM (21) to generate $P(r)$ curves.

RIα Heterodimers—To assess the general shape characteristics of RIα$_{AB}$·C heterodimers containing both Domains A and B, we measured the SAXS profiles of RIα$_{AB}$ and wild-type C-subunit complexes (Fig. 2*A*). The $P(r)$ functions for RIα$_{AB}$·C are similar to previous data from our laboratory (16), where a single peak with a maxima at 35 Å is followed by a long extended tail at the high r range. In the present experiments, the maximum dimension, D_{max} (105 Å), and R_g values (29.4 ± 0.1 and 32.4 ± 0.8 Å, from Guinier and GNOM analysis, respectively) are somewhat smaller than previously reported (D_{max} = 120–130 Å and R_g values = 36.4–38.6 Å) (16). These differences are most likely due to differences in sample handling or variations from one preparation to the next as was noted in our previous report (16). In the present study, we were careful to concentrate samples immediately prior to data collection to minimize possible aggregation.

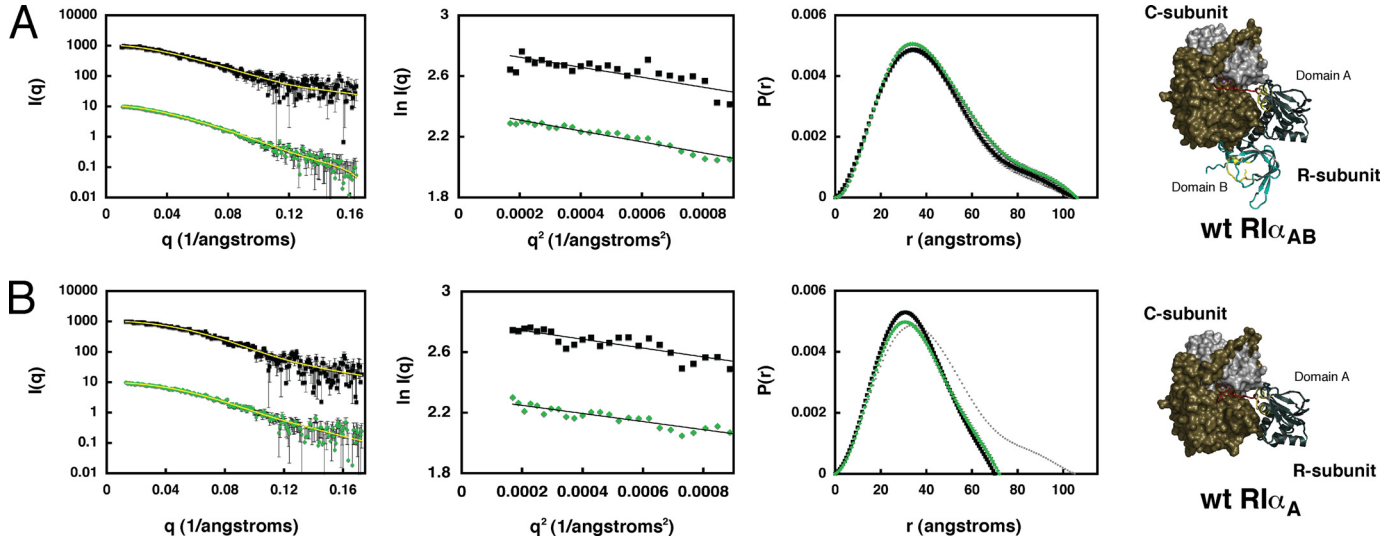

FIGURE 2. **SAXS profiles of RIα$_{AB}$ and RIα$_{A}$ heterodimers.** *A*, RIα$_{AB}$·C heterodimers. *B*, RIα$_{A}$·C heterodimers. *Left panels*, *I*(*q*) *versus q* plots. *Center panels*, Guinier plots. *Right panels*, *P*(*r*) curves calculated from x-ray scattering data. Heterodimers formed with wild-type C-subunit are shown in *black*, and heterodimers formed with C-subunit mutant K285P are shown in *green*. The *gray curve* in *B* is the *P*(*r*) function for RIα$_{AB}$·C for comparison. The intensity data in the *left* and *center panels* are in arbitrary units.

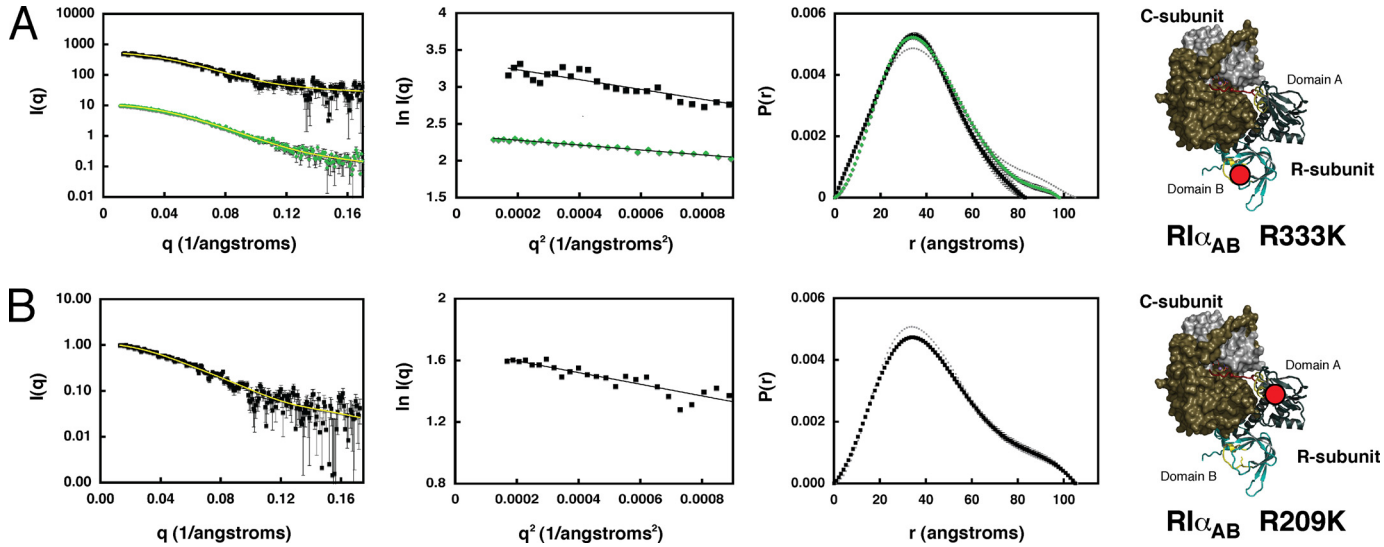

FIGURE 3. **SAXS profiles of RIα$_{AB}$ mutant heterodimers.** *A*, RIα$_{AB}$R333K·C heterodimers. *B*, RIα$_{A}$R209K·C heterodimers. *Left panels*, *I*(*q*) *versus q* plots. *Center panels*, Guinier plots. *Right panels*, *P*(*r*) curves calculated from x-ray scattering data. Heterodimers formed with wild-type C-subunit are shown in *black*, and heterodimers formed with C-subunit mutant K285P are shown in *green*. The *gray curves* are the *P*(*r*) function for RIα$_{AB}$·C from Fig. 1 for comparison. The intensity data in the *left* and *center panels* are in arbitrary units.

Effect of Deleting Domain B—To assess the contribution of Domain B to the overall shape of the heterodimer, we measured the x-ray scattering of a complex formed with RIα containing only one of the two cAMP-binding domains (RIα residues 91–244, RIα$_{A}$). This protein is the smallest fragment of RIα that still binds to both cAMP and the C-subunit with high affinity. The resulting *P*(*r*) function resembles a spherical, globular-shaped particle with a symmetrical Gaussian curve and no indication of the broad shoulder at the high *r* region detected in the RIα$_{AB}$·C complexes (Fig. 2*B*). The D_{max} measured by SAXS was 70 Å, consistent with the maximum dimensions determined from the crystal structure solved with the same constructs (29). In addition to differences in the *P*(*r*) curve, both the D_{max} and R_g values for RIα$_{A}$ are smaller than for RIα$_{AB}$ (Table 1). Thus, not only does Domain B contribute to the overall size of the complex, it also contributes to the broad shoulder observed in the RIα$_{AB}$·C *P*(*r*) function.

Effect of R333K on RIα Heterodimers—In contrast to the extended *P*(*r*) curve observed with the wild-type RIα$_{AB}$·C heterodimer, the *P*(*r*) function for the RIα$_{AB}$R333K·C heterodimer displays a Gaussian distribution typical of a globular, spherical particle (Fig. 3*A*). GNOM analysis reveals a *P*(*r*) function with a peak maximum at 35 Å that goes to zero at a D_{max} of 83 Å and an R_g value of 28.4 ± 0.4 Å (the R_g was estimated to be 28.3 ± 0.9 Å by Guinier analysis). The extended tail at the high *r* region in the RIα$_{AB}$·C heterodimer data is not detected in RIα$_{AB}$R333K·C. Both the D_{max} and R_g values are smaller for RIα$_{AB}$R333K·C complexes compared with RIα$_{AB}$ heterodimers without the R333K mutation. Moreover, PKA heterodimers formed with RIα$_{AB}$R333K

TABLE 1
Summary of SAXS data for PKA-Iα heterodimers

R-subunit	C-subunit	R_g		D_{max}[b]	V[c]
		Derived[a]	Calculated[b]		
		Å		Å	Å^3
$RI\alpha_{AB}$	C	29.4 ± 0.1	32.4 ± 0.8	105	157×10^3
$RI\alpha_{AB}$	C(K285P)	32.8 ± 0.04	34.1 ± 0.2	106	175×10^3
$RI\alpha_{A}$	C	26.5 ± 0.7	25.7 ± 0.2	70	92×10^3
$RI\alpha_{A}$	C(K285P)	27.3 ± 0.6	26.4 ± 0.2	72	116×10^3
$RI\alpha_{AB}$R333K (experimental)	C	28.3 ± 0.9	28.4 ± 0.4	83	133×10^3
$RI\alpha_{AB}$R333K (calculated)	C	NA[d]	28.8 ± 0.008	83	NA[d]
$RI\alpha_{AB}$R333K	C(K285P)	32.6 ± 0.6	31.44 ± 0.3	105	158×10^3
$RI\alpha_{AB}$R209K	C	33.5 ± 0.9	34.6 ± 0.4	105	155×10^3

[a] Derived using Guinier approximation.
[b] Calculated using the program GNOM.
[c] V is the molecular volumes calculated from DAMMIF. The expected dry volumes are calculated based on molecular mass and a partial specific volume of 0.073 cm^3/g. Hydration layer effects are expected to give rise to increases in the experimentally derived volumes.
[d] NA, not applicable.

resemble the more compact shapes observed with RII heterodimers (16).

The crystal structure of the PKA-Iα complex was solved using the R333K mutant, $RI\alpha_{AB}$R333K·C. We hypothesized that the R333K mutation trapped the R-subunit into a compact conformation enabling favorable crystal packing necessary to achieve crystals that diffract to <3 Å. To assess the validity of the crystallographically observed conformation in light of our solution scattering studies, we calculated the theoretical scattering intensities from atomic coordinates of the $RI\alpha_{AB}$R333K·C structure (Protein Data Bank code 2QCS) using the program CRYSOL (23) and generated a $P(r)$ function based on this theoretical scattering data. The experimental and calculated $P(r)$ curves are both very symmetrical without any significant tail at long r values (Fig. 4). Furthermore, both D_{max} and R_g values are in excellent agreement between the two data sets. Clearly, the experimental and calculated SAXS data closely overlap, confirming that the overall shape of the $RI\alpha_{AB}$R333K·C complex measured in solution is very consistent with what is observed in the crystal structure.

Based on the SAXS data of wild-type and $RI\alpha_{AB}$R333K·C heterodimers, the overall shape of these complexes are undoubtedly distinct (Fig. 3*A*). Although the $P(r)$ functions of wild-type $RI\alpha_{AB}$·C heterodimers have a broad tail at long vector lengths, both experimental and calculated $P(r)$ functions of $RI\alpha_{AB}$R333K·C heterodimers do not. The shoulder originates from Domain B because removal of this entire domain in $RI\alpha_{A}$·C complexes yield symmetrical $P(r)$ curves. Clearly, the overall shape of the wild-type heterodimer in solution as observed by SAXS is not consistent with the static image presented in the $RI\alpha_{AB}$R333K·C crystal structure. In solution, the wild-type $RI\alpha_{AB}$·C complex likely exists as an ensemble of conformational states ranging from compact to extended. The conformation observed in the crystal structure represents only one of many possible states available for the wild-type $RI\alpha_{AB}$·C heterodimer in solution. We propose that when bound to the C-subunit, the R333K mutation pushes the equilibrium state of RIα toward a dumbbell shape (Fig. 1*A*, *left panel*), resulting in a very compact R·C complex. The SAXS data suggest that in the absence of the R333K mutation, RIα is more dynamic and spends a significant fraction of time in an extended conformation.

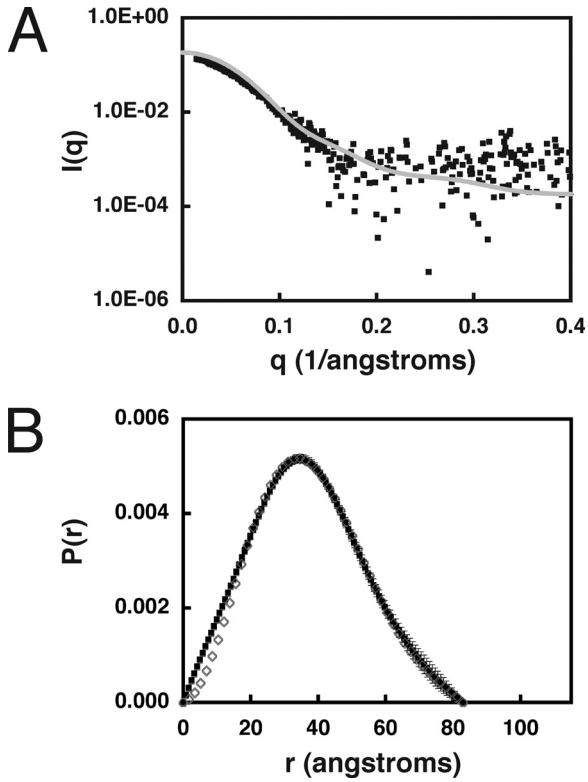

FIGURE 4. **Calculated scattering intensity from the $RI\alpha_{AB}$R333K·C heterodimer crystal structure.** *A*, calculated scattering intensity data using Protein Data Bank code 2QCS coordinates with the program CRYSOL (*gray*). The experimental data are shown in *black*. *B*, $P(r)$ functions of the experimental (*solid squares*) and calculated (*open diamonds*) data of $RI\alpha_{AB}$R333K·C heterodimers.

Effect of R209K on RIα Heterodimers—The R333K mutation impairs cAMP binding to Domain B, and the corresponding mutation for Domain A is R209K. To test whether this mutation also affects the dynamics of the R- and C-subunit interaction, we measured the x-ray scattering of R·C heterodimers formed with R209K. Unlike the R333K mutation, the $P(r)$ function for R209K·C shows little difference in the overall shape compared with the wild-type R·C heterodimer (Fig. 3*B*). The $P(r)$ function has a maximum peak at 34.7 Å, a D_{max} of 105 Å, and an R_g value of 34.6 ± 0.4 Å (33.5 ± 0.9 Å from Guinier analysis; Table 1). Clearly, the compaction of the R·C complex is specific only to the R333K mutation in Domain B.

Effect of the K285P Mutation on RIα Heterodimers—The PKA-Iα holoenzyme crystal structure defined a novel interaction site between Domain B of RIα and a short S-shaped loop (αH-αI loop) in the C-subunit (see Fig. 6, *A* and *B*) (11). The surface of each protein precisely complements the other at this site. Specifically, Domain B docks onto the C-subunit through side chain interactions between Asp^{276C}/Arg^{352R} and Thr^{278C}/Arg^{355R} in addition to backbone interactions between Lys^{285C} and both Arg^{355R} and Leu^{357R}. Mutation of Lys^{285} to proline reduced the ability of RIIβ to inhibit C-subunit activity (27), providing biochemical evidence that Domain B (in the R-subunit) and αH-αI loop (in the C-subunit) interaction site is important for at least the RIIβ isoform. Bioinformatics analysis has also pinpointed a short segment within the αH-αI loop (Gly^{282}–Gly^{286}) to be a conserved AGC kinase-specific insert (Fig. 6*B*, *left panel*) whose function has yet to be fully elucidated (31).

To specifically block Domain B in RIα from interacting with the C-subunit, we utilized the C-subunit mutation, K285P. To assess the effect of the K285P mutation on the solution structure of the $RI\alpha_{AB}$ heterodimer complex, we compared the x-ray scattering profiles of complexes formed with wild-type and mutant K285P C-subunits. Indeed, the *P*(*r*) functions of both $RI\alpha_{AB}$·C and $RI\alpha_{AB}$·C(K285P) complexes show very similar profiles where a single peak is followed by a long extended tail at the high *r* region (Fig. 2*A*). The maximum dimension of each complex was roughly the same (105 and 106 Å for wild-type and K285P C-subunits, respectively). Furthermore, the R_g values were similar for both proteins (32.4 and 34.1 Å for wild type and K285P, respectively).

We predicted that the x-ray scattering of R·C heterodimers formed with the $RI\alpha_A$ protein and the K285P mutant would be identical to wild-type C-subunit because the absence of Domain B in $RI\alpha_A$ eliminates the R-subunit interaction site with Lys^{285} in the C-subunit. Indeed, the *P*(*r*) functions are indistinguishable for $RI\alpha_A$ complexes formed with wild-type and K285P C-subunits (Fig. 2*B*).

For the $RI\alpha_{AB}$R333K·C heterodimer, we investigated whether the compact nature of the complex would be disrupted by interfering with the interaction site between Domain B and the large lobe of the C-subunit using the C(K285P) mutant. Indeed, the $RI\alpha_{AB}$R333K·C(K285P) double mutant complex no longer exhibits the compact symmetric *P*(*r*) curve observed with $RI\alpha_{AB}$R333K·C (Fig. 3*A*). Instead, the *P*(*r*) curve exhibits an extended tail at the high *r* region, similar to but not as pronounced as in the wild-type R·C heterodimer. Comparison of D_{max} and R_g parameters between wild-type and K285P heterodimers show remarkable overlap. Both the double mutant complex and wild-type heterodimer have a D_{max} of ~105 Å, and the R_g of the double mutant is 31.4 ± 0.3 Å compared with 32.4 ± 0.8 Å for $RI\alpha_{AB}$·C. SAXS scattering parameters for all wild-type and mutant R·C heterodimer complexes are summarized in Table 1. The inability of the K285P C-subunit mutant to fully recapitulate the solution structure of the wild-type R·C heterodimer probably indicates that the $RI\alpha_{AB}$R333K mutant still retains some effect on R·C interactions that prevents Domain B from exploring the full conformational space accessible to the wild-type $RI\alpha_{AB}$·C complexes.

TABLE 2
Association and dissociation rates of PKA-Iα and PKA-IIβ complexes (BIACORE)

R-subunit	C-subunit	K_a	K_d	K_D
		$M^{-1}s^{-1}$	s^{-1}	nM
$RI\alpha_{AB}$	C	91.9×10^4	8.44×10^{-4}	0.9
$RI\alpha_{AB}$	C(K285P)	90.6×10^4	44.3×10^{-4}	4.9
$RII\beta_{AB}$	C	11×10^4	3.16×10^{-4}	2.9
$RII\beta_{AB}$	C(K285P)	11×10^4	123×10^{-4}	111

Biochemical Analysis of RIα and RIIβ Heterodimers—The previous data show that the K285P mutant played a pivotal role in RIIβ inhibition of the C-subunit; however, the R·C binding constants were not measured (27). Given the differences in SAXS profiles between $RI\alpha_{AB}$·C and $RII\beta_{AB}$·C heterodimers, we postulated that the K285P mutation would not affect either the inhibition or binding affinities between RIα and the C-subunit.

Surface plasmon resonance was used to measure the binding constants between the R- and C-subunits. C-subunits were immobilized to CM5 chips by amine coupling, and $RI\alpha_{AB}$ was flowed across the chip surface. Compared with wild-type C-subunit, the K285P mutant exhibited a modest 5-fold decrease in binding affinity between the $RI\alpha_{AB}$ and C-subunits. The K_D was 4.9 nM for the K285P complex compared with 0.9 nM for the wild-type R·C complex (Table 2). In contrast, the K285P mutation caused a 38-fold decrease in binding affinity for the RIIβ·C heterodimer, where the K_D was 2.9 and 111 nM between RIIβ and wild-type C-subunit and C(K285P) mutant, respectively. The difference between the binding constants is solely attributed to differences in the dissociation rate.

We also used a ^{32}P incorporation protein kinase assay to measure the ability of RIα to inhibit both wild-type and mutant C-subunits. There was no statistically significant difference between wild-type and K285P C-subunit inhibition by RIα, where the IC_{50} was 2 ± 1 and 3 ± 1 nM, respectively (Fig. 5).

DISCUSSION

Proteins are in continuous motion, constantly sampling different conformations. Although crystallography provides high resolution information, this technique does not guarantee that the conformational state of the crystallized protein is representative of the predominant conformational state under physiological conditions and can be occasionally plagued by artificial conformations induced by crystal packing. To fully understand the intrinsic behavior of RIα·C complexes, solution techniques must also be utilized. In this study, we analyzed PKA-Iα heterodimers using a combination of SAXS and biochemical analysis to investigate domain dynamics within the protein complexes. SAXS is highly advantageous in that it provides low resolution structural information under a variety of solution-based physiological conditions and can be used to obtain size and shape information of large, highly dynamic proteins and protein complexes. Here, we compare our results to previous high resolution crystallographic data to obtain a more complete understanding of the large scale conformational dynamics of PKA. To explore the dynamics of Domain B in PKA-Iα holoenzyme complexes, we measured the equilibrium

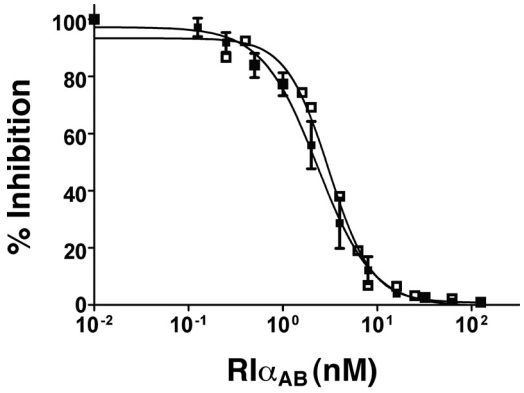

R-subunit	C-subunit	IC_{50} (nM)
$RI\alpha_{AB}$	C	2 ± 1
$RI\alpha_{AB}$	C (K285P)	3 ± 1
$RII\beta_{AB}$	C	4 ± 1*
$RII\beta_{AB}$	C (K285P)	16 ± 1*

FIGURE 5. **Inhibition of wild-type and K285P C-subunits by $RI\alpha_{AB}$.** Purified wild-type and K285P C-subunits were incubated with various concentrations of RIα-subunits. Catalytic activity was determined by measuring Kemptide phosphorylation via radioisotope [γ-^{32}P]ATP labeling. The data for wild-type C-subunit are shown as *solid squares*, and K285P mutant C-subunits are shown as *open squares*. The experiments were done in triplicate. The data for RIIβ are taken from Ref. 27 (*asterisks*).

R·C dissociation constants, the inhibition of the C-subunit by the R-subunit, and the overall shape of various mutant RIα·C complexes by small angle x-ray scattering. The most pronounced result of our study is that a single point mutation, R333K, alters the solution structural properties of PKA-Iα holoenzymes, presumably through effects on large scale dynamics of Domain B. The calculated x-ray scattering curve of the $RI\alpha_{AB}$R333K·C crystal structure is very consistent with our experimental SAXS results, indicating that the solution conformation of the $RI\alpha_{AB}$R333K·C heterodimer is very similar to what is observed in the $RI\alpha_{AB}$R333K·C crystal structure. Our SAXS data clearly indicate a large difference in the overall molecular shape between wild-type $RI\alpha_{AB}$·C and $RI\alpha_{AB}$R333K·C heterodimers. Differences in these solution structures likely arise from variations in domain dynamics within the two complexes, particularly with respect to Domain B. We postulate that Domain B in the $RI\alpha_{AB}$R333K·C heterodimer forms a stable interaction with the C-subunit via the αH-αI loop, but in wild-type RIα, Domain B interactions with the C-subunit are more transient, giving rise to the shoulder observed in the *P*(*r*) profiles.

The $RI\alpha_{AB}$R333K·C crystal structure revealed a previously unidentified single contact point between the αB helix in Domain B of RIα and the αH-αI loop in the C-subunit (Fig. 6*A*). We examined whether the interaction between the C-subunit αH-αI loop and the RIα Domain B observed crystallographically remains stable in solution or whether Domain B might have a more dynamic behavior in the PKA-Iα complex. Lys^{285} in the C-subunit αH-αI loop operates as a helix cap for the R-subunit αB helix (Fig. 6*B*, *right panel*), so we utilized the C-subunit mutation K285P as a strategy for disrupting the R·C interaction at the Domain B interface. K285P was first identified in a yeast genetic screen (32) and was shown to reduce the ability of RIIβ-subunits to inhibit C-subunit catalytic activity (27). If the interaction between Domain B (in RIα) and αH-αI loop (in the C-subunit) interface is stable as observed in the crystal structure, the K285P mutation would be expected to affect the overall shape characteristics in the $RI\alpha_{AB}$R333K·C complex. In contrast, if the Domain B interaction with the C-subunit in wild-type $RI\alpha_{AB}$·C complexes is *not* stable, the K285P should not affect the binding affinities or inhibition. Indeed for $RI\alpha_{AB}$·C(K285P) complexes, we found that K285P did not affect the general size or shape characteristics (Fig. 2) or inhibition by RIα (Fig. 5) and had only modest effects on the binding affinity (Table 2).

The only differences between K285P and wild-type C-subunit were seen in complexes formed with the $RI\alpha_{AB}$R333K mutant. The *P*(*r*) curve for the $RI\alpha_{AB}$R333K·C shows that it assumes the most compact shape of all the RIα complexes, which is presumably why crystallization of this complex (and not the wild type) was successful. SAXS analysis of $RI\alpha_{AB}$R333K·C(K285P) reveals a *P*(*r*) curve with a slightly extended tail at the high *r* region, but not to the large extent observed in $RI\alpha_{AB}$·C complexes. In other words, although the K285P mutation partially disrupted the interaction between Domain B and the C-subunit, it did not completely restore the full dynamic range of the wild-type heterodimer, suggesting that the average conformational state of Domain B in the $RI\alpha_{AB}$R333K·C(K285P) complex is intermediate between the fully compact form observed in the $RI\alpha_{AB}$R333K·C crystal and solution structures and the more extended $RI\alpha_{AB}$·C heterodimer solution structure.

The $RI\alpha_{AB}$R333K·C crystal structure highlights two additional ion pairs at the Domain B site: Asp^{276C}:Arg^{352R} and Thr^{278C}:Arg^{355R} (Fig. 6*B*, *right panel*). These two interactions may partially compensate for the release of the Lys^{285C}/Arg^{355R} and Lys^{285C}/Leu^{357R} interactions, thereby allowing for transient stabilization of Domain B against the C-subunit. The shoulder at 90–105 Å observed in the $RI\alpha_{AB}$·C *P*(*r*) curve likely stems from Domain B because the *P*(*r*) function becomes completely symmetrical upon removal of Domain B entirely in the $RI\alpha_{A}$·C complex (Fig. 2*B*). Given that the shoulder in the *P*(*r*) curve is only a small component, and the first peak at ~35 Å is the dominant component, the $RI\alpha_{AB}$·C complex is most likely a dynamic ensemble of conformational states where Domain B is mostly associated with the C-subunit but is detached from the C-subunit in a small fraction of complexes at any given time. This hypothesis is consistent with hydrogen-deuterium exchange mass spectrometry data where only 1 of 11 amides are protected in the αH-αI loop of the $RI\alpha_{AB}$·C complex (33).

Our SAXS results indicate that Domain B in RIα explores a large conformational space when bound to the C-subunit. Although the precise motion of Domain B within RIα·C complexes is not clear, we speculate that the flexibility stems from a hinge motion in some portion of the αB/C helix that connects the two cAMP-binding domains (Fig. 1). Analysis of various crystal structures demonstrates that RIα can adopt a large range of conformations. When RIα is bound to

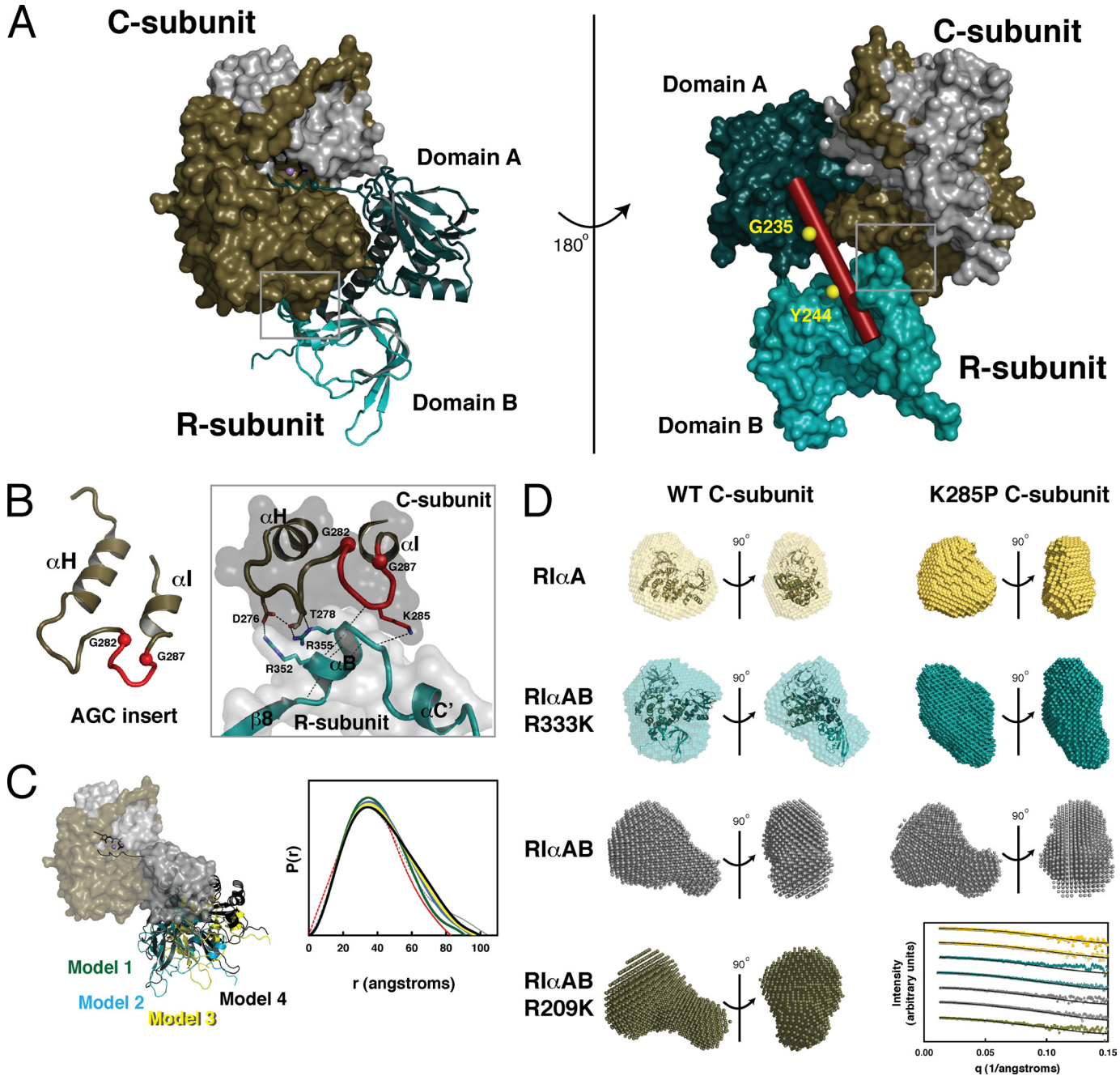

FIGURE 6. **Model of Domain B motions in the PKA-Iα complex.** *A*, crystal structure of the $RI\alpha_{AB}$R333K·C complex highlighting the interaction between RIα Domain B and the C-subunit (*gray box*). The small lobe of the C-subunit is in *white*, and the large lobe is in *brown*. The R-subunit Domain A is in *dark teal*, Domain B is in *light teal*, and the αB/C helix is depicted as a *red cylinder* in the *right panel*. *B*, *left*, the region between the αH-αI loop of the C-subunit (residues 282–287) is an insert specific to AGC kinases. *Right*, detailed illustration of the interaction between RIα Domain B and the C-subunit αH-αI loop. *C*, *left*, modeled movement of Domain B within the $RI\alpha_{AB}$·C complex. Domain B was rotated manually using residues Gly^{235} and Tyr^{244} as the hinge points. *Right*, simulated *P*(*r*) curves for the four different models. Theoretical scattering curves of each model were calculated using CRYSOL, and their corresponding *P*(*r*) curves were generated using GNOM. The experimental data for $RI\alpha_{AB}$R333K·C (*red*) and RIαAB·C (*gray*) are shown for comparison. *D*, averaged and filtered DAMMIF models for the seven PKA-Iα heterodimers. The DAMMIF models for $RI\alpha_{A}$·C and $RI\alpha_{AB}$R333K·C complexes are superimposed onto the crystal structure models (Protein Data Bank accession numbers 3FHI and 2QCS, respectively). The experimental scattering data (*colors*) were fit to the scattering curve calculated for the DAMMIF structure (*black*) in the *graph* in the *bottom right panel*. Wild-type (*WT*) C-subunit complexes are shown as *solid symbols*, and K285P C-subunit mutants are shown as *open symbols*. The colors for each curve are identical to colors for the DAMMIF models.

the C-subunit, the αB and αC helices are extended into one contiguous helix. When RIα is bound to cAMP, the same αB/αC helix is divided into three distinct helices separated by two bends at Gly^{235R} and Tyr^{244R}. There is a 22 Å difference in the maximum dimension between the most compact ($RI\alpha_{AB}$R333K·C) and the most extended ($RI\alpha_{AB}$·C) heterodimer, most likely because of hinge motions at the Gly^{235R} position. Gly^{235R} forms a hinge point at the C terminus of the αB helix (residues 226–235). This αB helix forms a hydrophobic interface with the C-subunit through Leu^{233R} and Met^{234R} in the R-subunit, and mutation of either residue permits activation of holoenzymes at lower cAMP concen-

trations,[3] suggesting that this region is strongly anchored to the C-subunit in wild-type proteins.

To test our hypothesis that hinge motions are responsible for the extended structures seen in the wild-type RIα$_{AB}$·C heterodimer, we took a computational approach and artificially introduced kinks at the Gly^{235R} and Tyr^{244R} hinge points of the RIα$_{AB}$R333K·C crystal structure and computed their scattering intensities and corresponding *P*(*r*) functions (Fig. 6*C*). Movement of Domain B away from the C-subunit resulted in larger R_g values, larger particle dimensions, and the presence of a shoulder at higher *r* values. Although the extended tail in these modeled *P*(*r*) functions is present in each curve, they are not as pronounced as the experimental data for the wild-type RIα$_{AB}$·C complex. Previous modeling of scattering data with the programs DAMMIN (34) and CONTRAST (35) do show that Domain B is positioned far from the C-subunit (16). Our efforts in computing *ab initio* three-dimensional shapes for each of the seven PKA-Iα mutant complexes resulted in an array of molecular structures (Fig. 6*D*). The DAMMIF results for the RIα$_{A}$·C complex resulted in the most globular shape and superimposed very well with the crystal structure model (Protein Data Bank code 3FHI). The RIα$_{AB}$R333K·C complex with the additional Domain B resulted in a compact structure as well and also superimposed very well with the crystal structure (Protein Data Bank code 2QCS). In contrast, the DAMMIF envelope predictions for the remaining complexes (RIα$_{AB}$·C, RIα$_{AB}$·C(K285P), RIα$_{AB}$R333K·C(K285P), and RIα$_{AB}$R209K·C) all exhibited elongated shapes. These results corroborate our hypothesis that in the wild-type R·C complex, Domain B in RIα is mobile in solution and samples an assortment of conformational states.

In light of data from other studies, it is apparent that the function of Domain B in RIα is not to provide high affinity binding to the C-subunit but to facilitate cAMP-dependent activation of the holoenzyme. Deletion of Domain B from RIα results in 500-fold higher concentrations of cAMP required to activate the holoenzyme and does not impair the ability of the remaining RIα structure to bind the C-subunit with high affinity (36). Similarly, preventing cAMP access to Domain B with the R333K mutation increases the activation constant for cAMP from 166 to >1500 nM (12). Collectively, these data are in agreement with the notion that Domain B is dispensable for stable RIα·C complex formation. Instead, the role of Domain B in RIα is to enhance activation of the RIα·C complex in response to cAMP.

From our data and others, it is unmistakable that the role of Domain B differs between RI- and RII-subunits. First, the activation of RIα·C is a stepwise process where cAMP must bind to Domain B before Domain A (12). For RIIβ, sequential binding of cAMP is not required for activation, where cAMP binding to either domain is sufficient to release catalytically active C-subunits (37). Second, Domain B contributes to high affinity binding between RIIβ$_{AB}$ and the C-subunit, but not between RIα$_{AB}$ and the C-subunit. Disruption of the interaction interface by the K285P mutation in the C-subunit resulted in a 38-fold decrease in K_D for RIIβ, *versus* a modest 5-fold decrease in K_D for RIα, suggesting that K285P is not critical for RIα·C complex formation but is significant for RIIβ·C formation. Third, previous studies demonstrated that the K285P mutation reduced the ability of RIIβ to inhibit the C-subunit and was sufficient to completely abolish BCY1 (the yeast homolog of mammalian RII subunits) inhibition of the C-subunit (27). Fourth, based on data from hydrogen/deuterium exchange-mass spectroscopy experiments, the αH-αI loop is well protected in the RIIβ·C complex (33, 37), whereas minimal protection is seen in the RIα·C complex (30). Lastly, SAXS analysis of the RIIβ·C complex shows a *P*(*r*) curve that reflects a compact particle (16), corroborating the view that Domain B forms a tight interaction with the C-subunit.

In this study, SAXS, in conjunction with mutagenesis and solution-based biochemical techniques, provides insights into domain dynamics within PKA complexes that are not feasible with x-ray crystallography alone. Taken together, our data suggest different roles of Domain B in RIα and RIIβ. For RIIβ, not only does Domain B interact tightly with the C-subunit, it is also necessary for inhibition of the C-subunit. In contrast, for RIα, Domain B is highly mobile, and its interaction with the C-subunit αH-αI loop is not necessary for inhibition, but Domain B *is* essential for the highly cooperative process of cAMP-dependent activation. Given the sequence and overall structural similarity between the four isolated R-subunit PKA isoforms, it is surprising that their dynamic behaviors differ in the context of holoenzyme complexes, giving rise to unique and sophisticated modes of cAMP-mediated activation. RI holoenzymes are finely tunable multimeric complexes that require a sequential series of events, unlike RII holoenzymes. Our investigation of protein dynamics in RI·C and RII·C heterodimers provides yet another layer of complexity that distinguishes the molecular features between PKA isoforms. From a global perspective, these structural distinctions give rise to the functionally nonredundant roles each isoform performs within the cell.

Acknowledgments—We thank Dr. Michael Deal (University of California, San Diego) for providing the C-subunit protein used in these studies and Dr. Dennis Winge (University of Utah) for performing the amino acid analyses. We also thank Jon Steichen for helpful discussions on the manuscript. We thank Dr. Jill Trewhella for the generous use of laboratory facilities at the University of Utah. X-ray scattering data were collected at the University of Utah using facilities that are supported by the United States Department of Energy Grant DE-FG02-05ER64026 (to Jill Trewhella).

REFERENCES

1. Arnsten, A. F., Ramos, B. P., Birnbaum, S. G., and Taylor, J. R. (2005) *Trends Mol. Med.* **11,** 121–128
2. Krebs, E. G., and Beavo, J. A. (1979) *Annu. Rev. Biochem.* **48,** 923–959
3. Chen, T. C., Hinton, D. R., Zidovetzki, R., and Hofman, F. M. (1998) *Lab. Invest.* **78,** 165–174
4. Amieux, P. S., Cummings, D. E., Motamed, K., Brandon, E. P., Wailes, L. A., Le, K., Idzerda, R. L., and McKnight, G. S. (1997) *J. Biol. Chem.* **272,** 3993–3998
5. Amieux, P. S., and McKnight, G. S. (2002) *Ann.* N. Y. *Acad. Sci.* **968,** 75–95
6. Groussin, L., Horvath, A., Jullian, E., Boikos, S., Rene-Corail, F., Lefebvre, H., Cephise-Velayoudom, F. L., Vantyghem, M. C., Chanson, P., Conte-Devolx, B., Lucas, M., Gentil, A., Malchoff, C. D., Tissier, F., Carney, J. A.,

[3] T. S. Sjoberg, C. Kim, A. P. Kornev, and S. S. Taylor, personal communication.

Bertagna, X., Stratakis, C. A., and Bertherat, J. (2006) *J. Clin. Endocrinol. Metab.* **91,** 1943–1949
7. Bertherat, J., Horvath, A., Groussin, L., Grabar, S., Boikos, S., Cazabat, L., Libe, R., René-Corail, F., Stergiopoulos, S., Bourdeau, I., Bei, T., Clauser, E., Calender, A., Kirschner, L. S., Bertagna, X., Carney, J. A., and Stratakis, C. A. (2009) *J. Clin. Endocrinol. Metabol.* **94,** 2085–2091
8. Horvath, A., Bossis, I., Giatzakis, C., Levine, E., Weinberg, F., Meoli, E., Robinson-White, A., Siegel, J., Soni, P., Groussin, L., Matyakhina, L., Verma, S., Remmers, E., Nesterova, M., Carney, J. A., Bertherat, J., and Stratakis, C. A. (2008) *Clin. Cancer Res.* **14,** 388–395
9. Dayal, A. K., and Kammer, G. M. (1996) *Arthritis Rheum.* **39,** 23–33
10. Kammer, G. M., Khan, I. U., and Malemud, C. J. (1994) *J. Clin. Investig.* **94,** 422–430
11. Kim, C., Cheng, C. Y., Saldanha, S. A., and Taylor, S. S. (2007) *Cell* **130,** 1032–1043
12. Herberg, F. W., Taylor, S. S., and Dostmann, W. R. (1996) *Biochemistry* **35,** 2934–2942
13. Murphy, C. S., and Steinberg, R. A. (1985) *Somat. Cell Mol. Genet.* **11,** 605–615
14. Steinberg, R. A., Russell, J. L., Murphy, C. S., and Yphantis, D. A. (1987) *J. Biol. Chem.* **262,** 2664–2671
15. Vigil, D., Blumenthal, D. K., Heller, W. T., Brown, S., Canaves, J. M., Taylor, S. S., and Trewhella, J. (2004) *J. Mol. Biol.* **337,** 1183–1194
16. Vigil, D., Blumenthal, D. K., Taylor, S. S., and Trewhella, J. (2005) *J. Biol. Chem.* **280,** 35521–35527
17. Vigil, D., Blumenthal, D. K., Taylor, S. S., and Trewhella, J. (2006) *J. Mol. Biol.* **357,** 880–889
18. Gullingsrud, J., Kim, C., Taylor, S. S., and McCammon, J. A. (2006) *Structure* **14,** 141–149
19. Herberg, F. W., Bell, S. M., and Taylor, S. S. (1993) *Protein Eng.* **6,** 771–777
20. Wu, J., Brown, S., Xuong, N. H., and Taylor, S. S. (2004) *Structure* **12,** 1057–1065
21. Svergun, D. (1992) *J. Appl. Crystallogr.* **25,** 495–503
22. Konarev, P. V., Volkov, V. V., Sokolova, A. V., Koch, M. H., and Svergun, D. I. (2003) *J. Appl. Crystallogr.* **36,** 1277–1282
23. Svergun, D., Barberato, C., and Koch, M. H. (1995) *J. Appl. Crystallogr.* **28,** 768–773
24. Franke, D., and Svergun, D. (2009) *J. Appl. Crystallogr.* **42,** 342–346
25. Volkov, V. V., and Svergun, D. (2003) *J. Appl. Crystallogr.* **36,** 860–864
26. Kozin, M. B., and Svergun, D. I. (2001) *J. Appl. Crystallogr.* **34,** 33–41
27. Yang, J., Kennedy, E. J., Wu, J., Deal, M. S., Pennypacker, J., Ghosh, G., and Taylor, S. S. (2009) *J. Biol. Chem.* **284,** 6241–6248
28. Prowse, C. N., Deal, M. S., and Lew, J. (2001) *J. Biol. Chem.* **276,** 40817–40823
29. Kim, C., Xuong, N. H., and Taylor, S. S. (2005) *Science* **307,** 690–696
30. Hamuro, Y., Anand, G. S., Kim, J. S., Juliano, C., Stranz, D. D., Taylor, S. S., and Woods, V. L., Jr. (2004) *J. Mol. Biol.* **340,** 1185–1196
31. Kannan, N., Haste, N., Taylor, S. S., and Neuwald, A. F. (2007) *Proc. Natl. Acad. Sci. U. S. A.* **104,** 1272–1277
32. Kennedy, E. J., Yang, J., Pillus, L., Taylor, S. S., and Ghosh, G. (2009) *PloS One* **4,** e4746
33. Anand, G. S., Hotchko, M., Brown, S. H., Ten Eyck, L. F., Komives, E. A., and Taylor, S. S. (2007) *J. Mol. Biol.* **374,** 487–499
34. Svergun, D. I. (1999) *Biophys. J.* **76,** 2879–2886
35. Heller, W. T., Abusamhadneh, E., Finley, N., Rosevear, P. R., and Trewhella, J. (2002) *Biochemistry* **41,** 15654–15663
36. Huang, L. J., and Taylor, S. S. (1998) *J. Biol. Chem.* **273,** 26739–26746
37. Zawadzki, K. M., and Taylor, S. S. (2004) *J. Biol. Chem.* **279,** 7029–7036